Re: DT12995
Cosmological constraints on the multiscalar field dark matter model
by L. O. T\'ellez-Tovar, Tonatiuh Matos, and J. Alberto V\'azquez

Dear Dr. Vazquez,

The above manuscript has been reviewed by one of our referees. Comments from the report appear below for your consideration.

When you resubmit your manuscript, please include a summary of the changes made and a brief response to all recommendations and criticisms.

Yours sincerely,

Dr. Panayiotis Tzanavaris (he/him/his)
Associate Editor
Physical Review D
Email: prd@aps.org
https://journals.aps.org/prd/
Follow us on Twitter @PhysRevD

NEWS FROM THE PHYSICAL REVIEW JOURNALS

PRX Energy is now open for submissions
https://go.aps.org/3lNdIqK

---

Second Report of the Referee -- DT12995/Tellez-Tovar

---

I am happy with the changes the authors have implemented. I recommend the paper
for publication.

I add a few minor comments on presentation that the authors can choose to implement. I believe it would help with the readability of the figures and add
clarity.

arXiv:2112.09337v1 [astro-ph.CO] 17 Dec 2021

# Cosmological constraints on the Multi Scalar Field Dark Matter model.

L. O. Téllez-Tovar,[1,2] Tonatiuh Matos,[1] and J. Alberto Vázquez[2,*]

[1] *Departamento de Física, Centro de Investigación y de Estudios Avanzados del IPN, A.P. 14-740, 07000 México D.F., México.*

[2] *Instituto de Ciencias Físicas, Universidad Nacional Autónoma de México, Apdo. Postal 48-3, 62251 Cuernavaca, Morelos, México.*

The main aim of this paper is to provide cosmological constraints on the Multi Scalar Field Dark Matter model (MSFDM), in which we assume the dark matter is made up of different ultra-light scalar fields. As a first approximation, we consider they are real and do not interact with each other. We study the equations for both the background and perturbations for $N$-fields and present the evolution of the density parameters, the mass power spectrum and the CMB spectrum. In particular, we focus on two scalar fields with several combinations for the potentials $V(\phi) = 1/2m_\phi^2\phi^2$, $V(\phi) = m_\phi^2 f^2\left[1+\cos(\phi/f)\right]$ and $V(\phi) = m_\phi^2 f^2\left[\cosh(\phi/f)-1\right]$, however the work, along with the code, can be easily extended to more fields. We use the data from BAO, Big Bang Nucleosynthesis, Lyman-$\alpha$ forest and Supernovae to find constraints on the sampling parameters for the cases of a single field and double field, along with the Bayesian evidence. We found that some combinations of the potentials get penalized through the evidence, however for others there is a preference as good as for the cold dark matter.

* javazquez@icf.unam.mx

## 1. INTRODUCTION

So far the most accepted cosmological model considers the contribution of cold dark matter (CDM) as a key component for structure formation, along with a cosmological constant ($\Lambda$), as the simplest form of dark energy. The success of this model, know as $\Lambda$CDM, relies mainly on the accurate agreement with several cosmological observations, for example measurements of the current accelerated expansion of the Universe and the Cosmic Microwave Background Radiation (CMB). The best description for the dark matter assumes to be made up of pressureless, non-relativistic, neutral and non-baryonic particles whose interaction is primarily through gravity. However, the assumption of a particle with these properties brings up many unexplained features, mainly at galactic scales, i.e. the central density behaviour in galactic halos or the overpopulation of substructures at small scales; for an extended review about the problems and possible solutions see Refs. [1, 2]. An alternative that may alleviate these problems is to consider a dark matter but now described by a single scalar field $\phi$ with an associated potential $V(\phi)$, whose evolution is carried out by the Klein-Gordon equation. The idea of assuming a scalar field as the Dark Matter (DM) of the Universe was introduced about two decades ago, where the simplest possibility is to be real, or complex, minimally coupled to gravity and interacting with ordinary matter only gravitationally [3–6]. Throughout the years, this model has been rediscovered and received many names, for example: Scalar Field DM (SFDM) [5], fuzzy DM [7], Bose-Einstein condensate DM [8] and, more recently, ultra-light axion DM [9], but a systematic study was carried out since [5]; here we will refer to it as SFDM, as it was named in [10]. Based on this idea, the particle associated to the field is an ultralight boson whose mass oscillates around $m_\phi \sim 10^{-22}$ eV and hence is able to form Bose-Einstein condensates that conform the galactic structures [9, 11–14]. In this work we will consider that the scalar field (or fields) are already formed and we will not delve into their origin; see Refs. [9, 15] for details.

For an expanding universe the scalar field cools down along with the expansion, and after a while, this causes that the field, the boson gas, freezes and then condensates. For an ideal boson gas the condensation temperature goes like $T_c \sim m^{-5/3}$, implying that for a mass big enough the condensation temperature becomes small, but the opposite happens if the mass turns out to be light, or ultra-light, the condensation temperature could be very high. However, after the turn around, the galaxies start forming and the re-collapse raises the temperature of the bosons again. Therefore, depending on the initial conditions of the galaxy formation, the boson particles can produce excited states, although most of the boson particles remain in the condensate state, or the ground state. These excited particles can be interpreted as other scalar fields. Thus, once the galaxy is already formed, if it still contains boson particles in several quantum states, then it can be interpreted as a galaxy with different scalar fields. On the other hand, for heavy particles these vibrations could be neglected, however for ultra-light particles an excitation could be comparable with its original mass. In an effective way the scalar field contains the mass plus the effective mass of the excitation's energy. Thus, this boson gas of particles in excited states could be seen effectively as many scalar fields with different potentials, hence the introduction of the Multi Scalar Field Dark Matter model.

Another motivation to introduce several scalar fields with different potentials could be encouraged because if the 4% of just the baryonic matter in the universe is so diverse, then we can suspect that the 26% of the matter, the dark matter, could be made of several species with different properties too. This diversity of particles could be observed and be tested at various scales, for instance at the galactic level by observing the rotation curves as well as at the largest scales of the Universe. If the dark matter is formed of scalar fields, then both results should match flawlessly. In this work we will focus on the largest scales of the Universe, letting for a parallel work the study of small scales [16].

It has been shown that a scalar field with a convex potential behaves, in average, like dust during late times and hence mimics the behaviour of the cold dark matter. However, depending on the specific form of the potential and even whether the field is real or complex, it may have different behaviors before acting like a pressure-less fluid. So, in order to have a dark matter evolution, it is necessary that the dependence of the potential with respect to the field is such that it presents a minimum value at some critical point around which the field oscillates [9, 14, 17]. Some examples of such kind of potentials are the parabolic function $V(\phi) = 1/2m_\phi^2\phi^2$ [12, 13, 18] and the self-interacting potential with a quartic term contribution $V(\phi) = 1/2m_\phi^2\phi^2 + \lambda_\phi\phi^4$ [15, 19–21], or the axion like potential $V(\phi) = m_\phi^2 f^2\,[1+\cos(\phi/f)]$ [22–24] and its analog $V(\phi) = m_\phi^2 f^2\,[\cosh(\phi/f) - 1]$ [25, 26]. Here $m_\phi$ is interpreted as the mass of the field, $\lambda_\phi$ is the self-interacting constant and $f$ represents a decay constant. For a single field, several constrictions on its mass have been imposed by using CMB and matter power spectrum [27], galactic dynamics [28], dwarf galaxies [29–31], $N$-body simulations with reionization process [32] and Lyman-$\alpha$ flux spectra [33, 34]. However, the presence of small inconsistencies among datasets are also found, and can be seen in Figure 1 of Ref. [15], and in Ref. [35]. This single field model provides a very good description of the evolution of the cosmological densities and the peaks of the CMB as well as the number of substructures in galaxy arrays, among others [9, 11–14]. Nonetheless it still presents some open issues [9]. For example, numerical simulations have shown that the mass of the field could vary for different scales of the simulation in order to fit the observations, for instance on the formation of galaxies [36], the whirling plane of satellite galaxies around the Milky Way, Andromeda and Centaurus A galaxies [37], or the same mass scale in satellite galaxies of the Milky Way [38], just to mention a few.

In this work, to alleviate these discrepancies, we open up the possibility that the dark matter may be composed of several types of scalar fields. That is, the main aim of this work is to present a model where the dark matter may be made up by several scalar fields, with different potentials, and to show its constraints imposed by current cosmological observations. This model may help us to alleviate the inconsistencies among the constrictions of the mass values obtained by different observations, arguing that they could be different dark matter particles [39]. Also, if we consider two scalar fields with different masses, the same mass scale in the satellite galaxies of the Milky Way could be explained, i.e. one type of particle could form the host galaxy and the other the satellites [40]. We will refer to this model as the Multi Scalar Field Dark Matter (MSFDM). Other areas have included similar ideas where two or more fields are used, for instance a combination of the inflaton and the SFDM [15], two scalar fields as dark energy [41, 42], the inflaton and the curvaton [43], two scalar fields for inflation [44, 45], interactions between dark energy and dark matter [46] or the axiverse model [39] (see also [47]).

Given the motivations above, in this paper we study the background dynamics and the linear perturbations of the model. As a first approximation we consider the scalar fields are spatially homogeneous, real and with no interaction among each other, however this part could be easily extended in future works. The paper is organized as follows: In sections 2.1 and 2.2 we present the equations for the background and linear perturbations. In section 2.3 the evolution is obtained with a modify version of the CLASS code for the background, mass power spectrum and CMB power spectrum for different combinations of potentials. In section 3 we show the model constraints, and finally in the last section we present our conclusions.

## 2. MATHEMATICAL BACKGROUND

### 2.1. Background dynamics

Throughout this paper we base our analysis on a flat Universe filled up with the standard components: baryons, dark energy in the form of a cosmological constant ($\Lambda$), photons and neutrinos as relativistic species and dark matter (DM). In particular, we assume the DM is described by multiple real scalar fields $\phi_i$ endowed with their corresponding potentials $V_i(\phi_i)$, whereas the rest of the matter components are modeled as perfect fluids. Assuming a Friedmann-Lemaitre-Robertson-Walker metric, the equations of motion for the background dynamics are

$$H^2 = \frac{\kappa^2}{2}\left(\sum_I \rho_I + \sum_i \rho_{\phi i}\right) , \tag{1a}$$

$$\dot{\rho_I} = -3\frac{\dot{a}}{a}\left(\rho_I + p_I\right) , \tag{1b}$$

$$\ddot{\phi_i} = -3H\dot{\phi_i} - \partial_{\phi i}V_i(\phi_i) . \tag{1c}$$

Here, dots represent derivatives with respect to the cosmic time $t$, $H$ is the Hubble parameter, $\kappa^2 = 8\pi G$, and $\rho_I$ and $p_I$ are the energy density and pressure of the $I$-th fluid species respectively, whereas for the scalar fields we have the associated density and pressure given by the standard expressions

$$\rho_{\phi i} = (1/2)\dot{\phi_i}^2 + V_i(\phi_i), \qquad p_{\phi i} = (1/2)\dot{\phi_i}^2 - V_i(\phi_i). \tag{2}$$

Notice that we are assuming different species of scalar fields, represented each one by the subindex $i$ in the above equations. The Klein-Gordon equations (1c), for each of the fields, can be written in a more manageable form by using the following polar transformation [48]

$$\frac{\kappa\dot{\phi_i}}{\sqrt{6}H} \equiv \Omega_{\phi i}^{1/2}\sin(\theta_i/2) , \quad \frac{\kappa V_i^{1/2}}{\sqrt{3}H} \equiv \Omega_{\phi i}^{1/2}\cos(\theta_i/2) , \tag{3a}$$

where $\Omega_{\phi i} \equiv \kappa^2\rho_{\phi i}/3H^2$ represents the dimensionless density parameter, and similarly $\theta_i$ is an angular degree of freedom directly related to the equation of state (EoS) for each one of the fields, $w_{\phi i} \equiv p_{\phi i}/\rho_{\phi i} = -\cos\theta_i$. Additionally, we define the potential variables $y_{1i}$ and $y_{2i}$ as

$$y_{1i} \equiv -2\sqrt{2}\frac{\partial_{\phi i}V_i^{1/2}}{H} , \quad y_{2i} \equiv -4\sqrt{3}\frac{\partial^2_{\phi i}V_i^{1/2}}{\kappa H} , \tag{3b}$$

whose form depend on the potential for a particular field.

As a proof of the concept, we focus our study on the following potentials

$$V_i(\phi_i) = \begin{cases} m_{\phi i}^2 f_i^2\left[1+\cos(\phi_i/f_i)\right] & \cos \\ (1/2)m_{\phi i}^2\phi_i^2 & \text{quadratic} \\ m_{\phi i}^2 f_i^2\left[\cosh(\phi_i/f_i)-1\right] & \cosh \end{cases} . \tag{4}$$

and their possible combinations; with $f_i$ being a characteristic energy scale for the scalar fields $\phi_i$, and $m_{\phi i}$ its corresponding mass scale. It can be seen that the variables (3b) for the aforementioned potentials can be written as

$$y_{1i}^2 = 4\frac{m_{\phi i}^2}{H^2} - 2\lambda_{\phi i}\Omega_{\phi i} , \tag{5a}$$

$$y_{2i} = \lambda_{\phi i}y_{1i} . \tag{5b}$$

Notice that each of the three functional forms in (4) can be selected from a given dimensionless parameter, $\lambda_{\phi i} = 3/\kappa^2 f_i^2$, which facilitates the numerical calculations. Positive values of $\lambda_{\phi i} > 0$ describe the cosine potential and negative ones $\lambda_{\phi i} < 0$ the cosh potential, whereas the quadratic case corresponds to $\lambda_{\phi i} = 0$ (for more details see [18, 22, 26]). Then, for each field, the associated Klein-Gordon equation (1c) is represented by the following set of coupled equations

$$\theta_i' = -3\sin\theta_i + y_{1i}\,, \tag{6a}$$

$$\Omega_{\phi i}' = 3\left(w_{tot} + \cos\theta_i\right)\Omega_{\phi i}\,, \tag{6b}$$

$$y_{1i}' = \frac{3}{2}\left(1 + w_{tot}\right)y_{1i} + \frac{1}{2}\lambda_{\phi i}\Omega_{\phi i}^{1/2}\sin\theta_i\,, \tag{6c}$$

with $w_{tot} = \sum_I \Omega_I w_I + \sum_i \Omega_i w_i$, where $\Omega_I \equiv \kappa^2\rho_I/3H^2$ and $w_I = p_I/\rho_I$. The prime denotes derivative with respect to the number of e-folds $N = \ln a$, and for any given variable $q$ we have the relation $\dot{q} = Hq'$.

The initial conditions necessary to solve these equations can be seen in Eq. (2.16) of Ref. [18] for the quadratic case, for the cosine potential see Eq. (5) Ref. [22] and for the hyperbolic cosine see Eq. (2.6) in Ref. [26]. The main purpose in all cases is to match a given value of the density parameter $\Omega_{\phi i,0}$ at the present time with the initial values of the dynamical quantities $(\theta_i, y_{1i}, \Omega_{\phi i})_{\rm ini}$ at early enough times (typically for a scale factor of the order of $a_{\rm ini} \simeq 10^{-14}$).

In general terms, the mass parameter $m_{\phi i}$ determines the start of the rapid oscillations of the field $\phi_i$ around the minimum of the potential $V_i$, which happens at around $H \simeq 3m_{\phi i}$. For $\lambda_{\phi i} \neq 0$, Eq. (5a) becomes a constraint equation that must be satisfied by the field variables at all times, whereas for $\lambda_{\phi i} = 0$ it simply tells us that $y_{1i} = 2m_{\phi i}/H$. In fact, one expects that at late times $m_{\phi i} \gg H$ so that for the three cases in (4) the relation $y_{1i} = 2m_{\phi i}/H$ should be satisfied with high accuracy. Only for the case $\lambda_{\phi i} < 0$ (cosh potential) it is also necessary to impose the scaling solution during radiation domination: $\Omega_{\phi i} = -12/\lambda_{\phi i}$ and $\cos\theta_i = -1/3$, and then the initial value of $y_{1i}$ is calculated from Eq. (5a). Furthermore, the field mass $m_{\phi i}$ is not an independent parameter in this case, and it has been shown that the two parameters are related through [26]

$$\frac{m_{\phi i}}{H} = 1.5\left[\left(\frac{\lambda_{\phi i}}{3} - 4\right)\frac{\Omega_{\phi i,0}}{\Omega_{r,0}}a_{\rm ini}\right]\,, \tag{7}$$

with $\Omega_{r,0}$ the present density parameter of relativistic species and $a_{\rm ini}$ the initial value of the scale factor.

### 2.2. Linear density perturbations

We consider the linear perturbations for the scalar fields by expanding the field to the leading order, with $\phi_i\left(\vec{x},t\right) = \phi_i\left(t\right) + \varphi_i\left(\vec{x},t\right)$, where $\phi_i(t)$ are the background fields described in the above section, whereas $\varphi_i$ are the field linear perturbations. The perturbed metric, in the synchronous gauge is $ds^2 = -dt^2 + a^2(t)\left(\delta_{lm} + h_{lm}\right)dx^l dx^m$, with $h_{lm}$ being the tensor perturbations of the metric. Working in Fourier space, the perturbed Klein-Gordon equation for each field is given by

$$\ddot{\varphi}_i = -3H\dot{\varphi}_i - \left(\frac{k^2}{a^2} + \partial_{\phi i}^2 V_i\right)\varphi_i - \frac{1}{2}\dot{h}\dot{\phi}_i\,. \tag{8}$$

In Eq. (8), $k$ is the comoving wavenumber, $h$ is the trace of $h_{lm}$ and $\dot{h}$ is known as the metric continuity. Following the idea presented for the background in the previous section, we use the

polar variables [18, 22],

$$\sqrt{\frac{2}{3}}\frac{\kappa\dot{\varphi}_i}{H} = -\Omega_{\phi i}^{1/2} e^{\alpha_i}\cos\left(\frac{\vartheta_i}{2}\right), \qquad \frac{\kappa y_{i,1}\varphi_i}{\sqrt{6}} = -\Omega_{\phi i}^{1/2} e^{\alpha_i}\sin\left(\frac{\vartheta_i}{2}\right), \tag{9}$$

where $\alpha_i$ and $\vartheta_i$ are the new perturbation quantities. If we define the new quantities

$$\delta_{0i} = -e^{\alpha_i}\sin\left(\frac{\theta_i - \vartheta_i}{2}\right), \qquad \delta_{1i} = -e^{\alpha_i}\cos\left(\frac{\theta_i - \vartheta_i}{2}\right), \tag{10}$$

where the density contrast is $\delta_{\phi i} \equiv \delta\rho_{\phi i}/\rho_{\phi i} = \delta_{0i}$, then the perturbed Klein-Gordon equation (8) can be rewritten as

$$\delta_{0i}' = -\left[3\sin\theta_i + \frac{k^2}{k_{Ji}^2}(1-\cos\theta_i)\right]\delta_{1i} + \frac{k^2}{k_{Ji}^2}\sin(\theta_i)\,\delta_{0i} - \frac{1}{2}h'(1-\cos\theta_i), \tag{11a}$$

$$\delta_{1i}' = -\left[3\cos\theta_i + \left(\frac{k^2}{k_{Ji}^2} - \frac{\lambda_{\phi i}\Omega_{\phi i}}{2y_{1i}}\right)\sin\theta_i\right]\delta_{1i} + \left(\frac{k^2}{k_{Ji}^2} - \frac{\lambda_{\phi i}\Omega_{\phi i}}{2y_{1i}}\right)(1+\cos\theta_i)\,\delta_{0i} - \frac{1}{2}h'\sin\theta_i, \tag{11b}$$

where we have introduced the Jeans wavenumber as $k_{Ji}^2 = H^2a^2y_{1i}$. Other quantities of interest are the perturbations for the energy density $\delta\rho_{\phi i}$, pressure $\delta p_{\phi i}$ and velocity divergence $\Theta_{\phi i}$, which are explicitly read

$$\delta\rho_{\phi i} = \dot{\phi}_i\dot{\varphi}_i + \partial_{\phi i}V\varphi_i, \tag{12a}$$

$$\delta p_{\phi i} = \dot{\phi}_i\dot{\varphi}_i - \partial_{\phi i}V\varphi_i, \tag{12b}$$

$$(\rho_{\phi i} + p_{\phi i})\,\Theta_{\phi i} = \frac{k^2}{a}\dot{\phi}_i\varphi_i. \tag{12c}$$

In terms of the new variables $\delta_{0i}$ and $\delta_{1i}$, they are written as

$$\delta\rho_{\phi i} = \delta_{0i}\,\rho_{\phi i}, \tag{13a}$$

$$\delta p_{\phi i} = (\delta_{1i}\sin\theta_i - \delta_{0i}\cos\theta_i)\;\rho_{\phi i}, \tag{13b}$$

$$(\rho_{\phi i} + p_{\phi i})\,\Theta_{\phi i} = \frac{k^2\rho_{\phi i}}{aHy_{i,1}}\left[(1-\cos\theta_i)\,\delta_{1i} - \sin\theta_i\delta_{0i}\right]. \tag{13c}$$

Again, depending on the value of $\lambda_{\phi i}$, one recovers the perturbed equations of any of the three different potentials of this work (4). The initial conditions for the perturbations simply are $\delta_{0\text{init}} = 0$ and $\delta_{1\text{init}} = 0$. It has been shown that the dynamical variables $\delta_{0i}$ and $\delta_{1i}$ quickly reach an attractor behavior driven by the non-homogeneous term $h'$ in Eqs. (11) [18, 22, 26].

### 2.3. Numerical Results

In this section we show the background evolution, mass power spectrum (MPS) and CMB power spectrum for different combinations of potentials, obtained with a modified version of the CLASS code that is able to deal with multiple scalar fields [18, 22, 50]. This version of the code is publicly available and can be found in [51]. We use the ratio $R = \Omega_{\phi 1,0}/\Omega_{\text{DM},0}$[1] to parameterize the energy density of the scalar fields, where $\Omega_{\text{DM},0} = \Omega_{\phi 1,0} + \Omega_{\phi 2,0} + \Omega_{\text{cdm},0}$ represents the current total dark matter contribution from the scalar fields sector. The mass values for the fields were taken from the references mentioned in the introduction, in particular, those reported in [40].

[1] The combination of the fields is symmetric, then for reference we take $\phi_1$ to define $R$, otherwise if $\phi_j$ is taken as reference we need to redefine $R = \Omega_{\phi j}/\left(\sum_i \Omega_{\phi i} + \Omega_{\text{cdm}}\right)$.

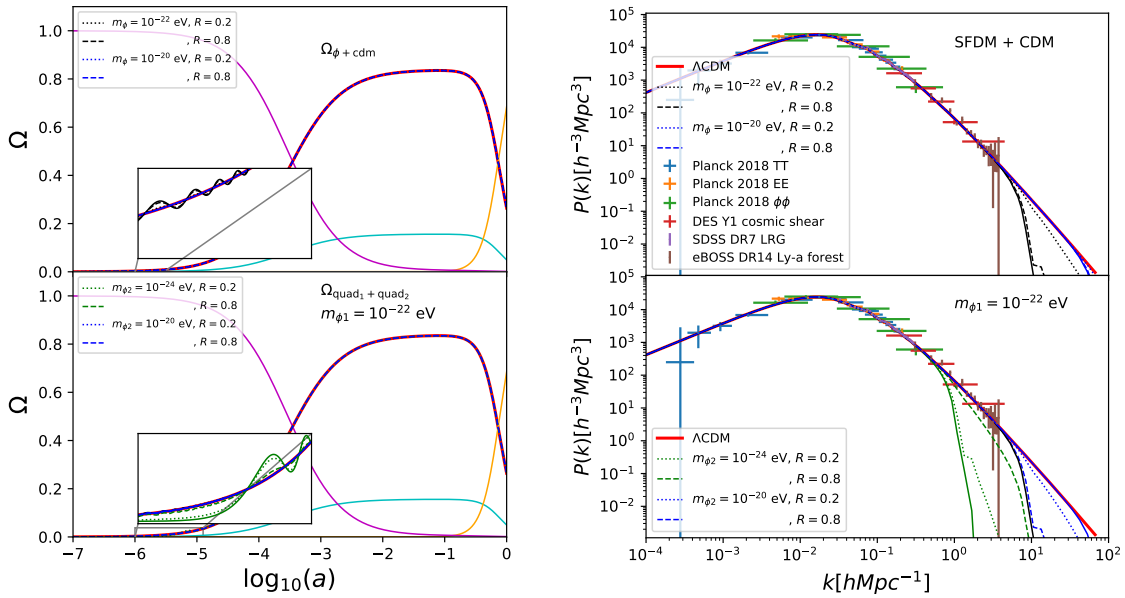



FIG. 1. Evolution of the density parameters $\Omega$ (left) and the linear matter power spectrum (right) at $z = 0$, for a SFDM + CDM model (top) and double field model (bottom). The field potential in all cases is the quadratic one $V(\phi) = \frac{1}{2}m_\phi^2\phi^2$, and $R$ represents the ratio of the field contribution to the total DM. The red, cyan, orange and magenta solid curves represent CDM, baryons, dark energy and relativistic species, respectively. As reference, the green, black and blue solid lines represent the evolution for a single scalar field with quadratic potential for $m_\phi = 10^{-24}$, $10^{-22}$ and $10^{-20}$ eV respectively. The data points for the MPS were obtained from [49].

Throughout this work we consider several combinations for the fields, and combined them with the CDM as well. This is because, until now, the nature of the dark matter is not yet determined and several possibilities should bear in mind. As the next approximation to the single field, here we assume two types of fields with different combinations of potentials as dark matter, however, once we have enough accurate data, the analysis (and the code) could be easily generalized to $N$ different fields.

In the first combination we assume the field one has $V(\phi_1) = \frac{1}{2}m_{\phi 1}^2\phi_1^2$ while the rest of the dark matter density is conformed by CDM, therefore $\Omega_{\phi 2,0} = 0$. As we can see on the upper left panel of Figure 1, the main difference in the background is the start of the scalar field oscillations due to the mass and $R$ values. If $R > 0.5$ the oscillations approach those of a single scalar field while if $R < 0.5$ the oscillations are less evident until they disappear when $R = 0$ (there is only CDM). In the mass power spectrum, the upper right panel of the same figure, we notice the expected cut-off in small scales for the lightest mass values ($m_{\phi 1} < 10^{-20}$ eV) but the behaviour is lost for heavier masses ($m_{\phi 1} > 10^{-20}$ eV) because the scalar field behaves like dust. Similar to the background, we found that the MPS of the combinations is bounded by the cases $R = 1$ (only SFDM) and $R = 0$ (only CDM). We can see an example of this in the upper panel of Figure 1 for $m_{\phi 1} = 10^{-22}$ eV (black line) and $10^{-20}$ eV (blue line) with $R = 0.2$ (dotted) and $R = 0.8$ (dashed). For $R = 0.8$ the oscillations approach the case of a single SFDM but disappear for $R = 0.2$, this is evident for $m_{\phi 1} = 10^{-22}$ eV. In the same way, in the right panel, when $R = 0.8$ the mass power spectrum shows a cut-off similar to the single case for both values $m_{\phi 1} = 10^{-22}$ and $10^{-20}$ eV, but it behaves like CDM (red solid line) for $R = 0.2$.

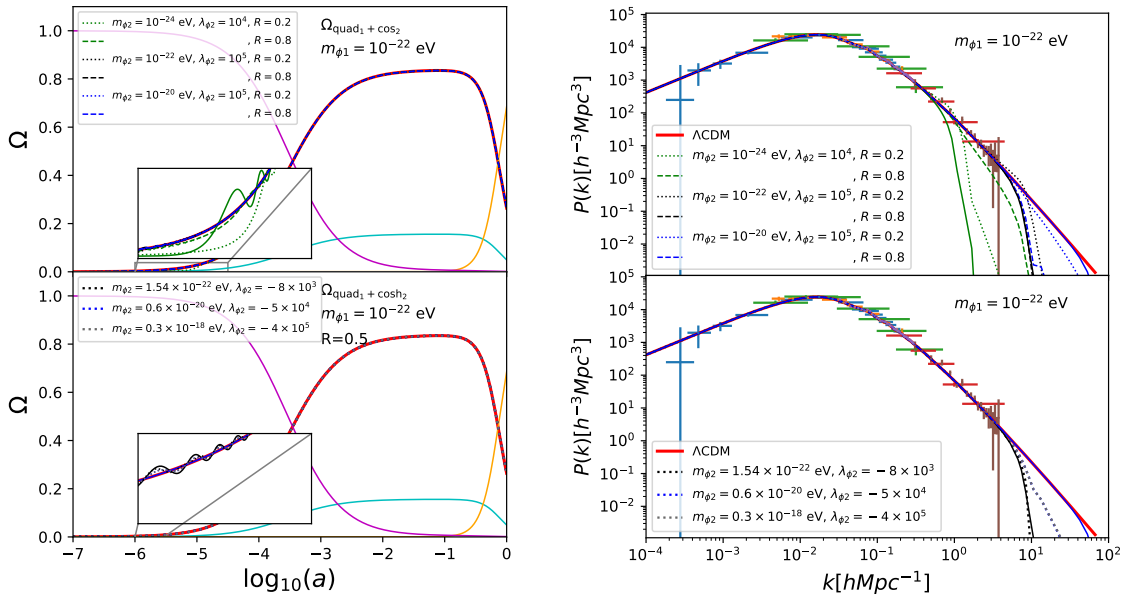



FIG. 2. Evolution of the density parameters $\Omega$ (left) and the linear matter power spectrum (right) at $z = 0$, for a model with two fields. Here, in both cases the field one has the same potential $V(\phi) = \frac{1}{2}m_\phi^2\phi^2$ with mass value $m_\phi = 10^{-22}$ eV as reference. However, in the top row, the second field has $V(\phi_2) = m_{\phi2}^2 f^2\,[1+\cos(\phi_2/f)]$ while in the lower row it has $V(\phi_2) = m_{\phi2}^2 f^2\,[\cosh(\phi_2/f)-1]$. The red, cyan, orange and magenta solid curves represent CDM, baryons, dark energy and relativistic species, respectively. As reference, the green, black and blue solid lines represent the evolution for a single scalar field with quadratic potential for $m_\phi = 10^{-24}$, $10^{-22}$ and $10^{-20}$ eV respectively. The data points for the MPS were obtained from [49].

For the second combination we assume two scalar fields with no CDM, both of them with a quadratic potential $V(\phi_{1,2}) = \frac{1}{2}m_{\phi1,2}^2\phi_{1,2}^2$ (lower panel of Fig. 1). We found that the total contribution to the background evolution, in particular the oscillations of the fields, depends on the contribution of each one through $R$ and are bounded by the oscillations of the lightest and the heaviest field respectively. For the MPS, the cut-off is more evident when the lightest field accounts for the principal contribution to $\Omega_{\rm DM,0}$ ($m_{\phi2} > m_{\phi1}$ and $R > 0.5$ or $m_{\phi2} < m_{\phi1}$ and $R < 0.5$), the behavior is closer to single field models ($R = 0$ or $R = 1$) depending of the dominant field, as expected. In the lower left panel of Figure 1 we show the total contribution of the fields to the background using $m_{\phi1} = 10^{-22}$ eV with $m_{\phi2} = 10^{-24}$ eV (green). The oscillations are more evident for $R = 0.8$ (dashed) than for $R = 0.2$ (dotted) and both of them are bounded by the single cases (solid). This is seen as well, but it is less noticeable due to the masses values, for the combination $m_{\phi1} = 10^{-22}$ eV with $m_{\phi2} = 10^{-20}$ eV (blue). For the MPS, we use the same values and we find a behavior similar to the previous case.

We also study a third combination of double field but now with $V(\phi_1) = \frac{1}{2}m_{\phi1}^2\phi_1^2$ and $V(\phi_2) = m_{\phi2}^2 f^2\,[1+\cos(\phi_2/f)]$ respectively. For the background we observe a similar behavior than in the previous combinations, that is, once we kept the masses fixed and solely modify the $\lambda_{\phi2}$ values, we see no difference among them. The oscillations of the fields depend on the masses and $R$, similarly to the quadratic potentials case. See, for example, the upper panel in Figure 2 where we take $m_{\phi1} = 10^{-22}$ eV along with $m_{\phi2} = 10^{-24}$ eV with $\lambda_{\phi2} = 10^4$ (green), $m_{\phi2} = 10^{-22}$ eV with $\lambda_{\phi2} = 10^5$ (black) and $m_{\phi2} = 10^{-20}$ eV with $\lambda_{\phi2} = 10^5$ (blue) for $R = 0.2$ (dotted) and $R = 0.8$ (dashed). For the MPS we see differences depending on $m_{\phi1,2}$ values or $R$ and also by

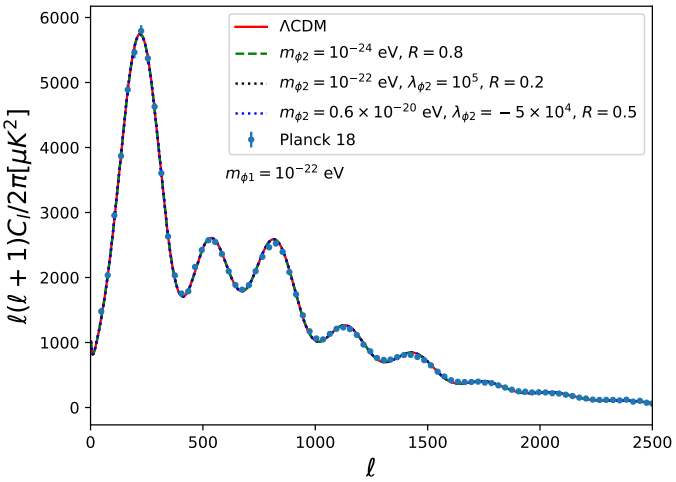



FIG. 3. The CMB power spectrum for $V(\phi_{1,2}) = \frac{1}{2}m^2_{\phi 1,2}\phi^2_{1,2}$ (green dashed line), $V(\phi_1) = \frac{1}{2}m^2_{\phi 1}\phi^2_1$ with $V(\phi_2) = m^2_{\phi 2}f^2\left[1+\cos(\phi_2/f)\right]$ (black dotted line) and $V(\phi_1) = \frac{1}{2}m^2_{\phi 1}\phi^2_1$ with $V(\phi_2) = m^2_{\phi 2}f^2\left[\cosh(\phi_2/f)-1\right]$ (blue dotted line). Solid red line represents the CMB for ΛCDM.

varying $\lambda_{\phi 2}$ values. In order to see a bump in the MPS we need that the second field dominates ($R < 0.5$) with lighter mass and higher $\lambda_{\phi 2}$. In the right side of the upper panel in Figure 2 we can see the bump before the cut-off for the green and black dotted lines, because in both cases the second field dominates and $\lambda_{\phi 2}$ has high values with lighter masses. On the other hand, in the blue dotted line we do not observe the bump yet because the field is too heavy ($m_{\phi 2} \geq 10^{-20}$ eV).

Finally, we study the combination of the field potential $V(\phi_1) = \frac{1}{2}m^2_{\phi 1}\phi^2_1$ with $V(\phi_2) = m^2_{\phi 2}f^2\left[\cosh(\phi_2/f)-1\right]$. In the background and MPS we have a similar behavior as before. This can be seen in the lower panel of Figure 2 where we take the combination $m_{\phi 1} = 10^{-22}$ eV, $m_{\phi 2} = 1.54 \times 10^{-22}$ eV, $\lambda_{\phi 2} = -8 \times 10^3$ (black), $m_{\phi 1} = 10^{-22}$ eV, $m_{\phi 2} = 0.6 \times 10^{-20}$ eV, $\lambda_{\phi 2} = -5 \times 10^4$ (blue) and $m_{\phi 1} = 10^{-22}$ eV, $m_{\phi 2} = 0.3 \times 10^{-18}$ eV, $\lambda_{\phi 2} = -4 \times 10^4$ (gray). It is important to note that both fields have the same contribution ($R = 0.5$), other combinations require further analysis. In the mass power spectrum, at small scales, we see that $\lambda_{\phi 2}$ has a greater contribution compared to the previous case because for the cosh-like potential the scalar field mass depends on the $\lambda_{\phi 2}$ value, contrary to the cos-like potential in which these parameters are independent. When $m_{\phi 2} \sim m_{\phi 1}$ we can appreciate a different behavior depending on the value of $\lambda_\phi$, for example, the black dotted line. However, if $m_{\phi 2} \geq m_{\phi 1}$, the change in $\lambda_{\phi 2}$ does not display noticeable changes (blue dotted and gray dotted lines).

In general, throughout the analysis we found a cut-off at small scales in the mass power spectrum that differentiates our model from the CDM.

Regarding the CMB spectrum, when the mass of at least one of the fields, for any combination, is less than $m_{\phi i} < 10^{-26}$ eV, the spectrum of the fields differs from the ΛCDM spectrum. However, for masses greater than $m_{\phi i} > 10^{-26}$ eV the same CMB power spectrum is obtained as for ΛCDM regardless of the value of $\lambda_\phi$ or $R$. See, for example Figure 3 where we show the CMB power spectra for $V(\phi_{1,2}) = \frac{1}{2}m^2_{\phi 1,2}\phi^2_{1,2}$ with $m_{\phi 1} = 10^{-22}$ eV, $m_{\phi 2} = 10^{-24}$ eV and $R = 0.8$ (green dashed line); $V(\phi_1) = \frac{1}{2}m^2_{\phi 1}\phi^2_1$ with $V(\phi_2) = m^2_{\phi 2}f^2\left[1+\cos(\phi_2/f)\right]$ for $m_{\phi 1} = 10^{-22}$ eV, $m_{\phi 2} = 10^{-22}$ eV, $\lambda_{\phi 2} = 10^5$ and $R = 0.2$ (black dotted line) and $V(\phi_1) = \frac{1}{2}m^2_{\phi 1}\phi^2_1$ with $V(\phi_2) = m^2_{\phi 2}f^2\left[\cosh(\phi_2/f)-1\right]$ for $m_{\phi 1} = 10^{-22}$ eV, $m_{\phi 2} \propto 10^{-20}$ eV, $\lambda_{\phi 2} = -5 \times 10^4$ and $R = 0.5$ (blue dotted line). For the three cases we have obtained nearly the same CMB power spectra as for the ΛCDM model (solid

red line). We also plotted the Planck-18 dataset as reference.

## 3. COMPARISON WITH DATA

In this section we present the Bayesian inference procedure in order to constrain the MSFDM models by using different data sets. We first perform the cosmological analysis and then discuss the merits of the models with respect to CDM within the framework of the Bayesian model selection.

### 3.1. Cosmological constraints

In the previous section we saw that the main difference throughout the models rests on the mass power spectrum at small scales, hence we use the Lyman-$\alpha$ 3D matter power spectrum data from BOSS and eBOSS collaboration [49][2]. We also use the Ly-$\alpha$ BAO from eBOSS DR14 [52], the Galaxy BAO from DR12 [53], 6dFGS [54] and SDSS DR7 [55], and the SNe Ia survey Pantheon [56] to improve the constraining power.

The flat priors used for the sampling parameters are as follow[3]: $H_0 = [10, 100]$ for the Hubble constant in km $s^{-1}Mpc^{-1}$, $\Omega_{\phi 1,0} = \Omega_{\phi 2,0} = [0, 1]$ for the scalar fields density parameters today, $\omega_{b,0} = [0.005, 0.1]$ for the physical baryon density, $\log_{10}(m_{\phi i}/\mathrm{eV}) = [-24, -17]$ for the scalar fields masses, $\log_{10}(\lambda_{\phi i}) = [1, 6]$ for the parameter on the trigonometric cosine potential and $\lambda_{\phi i,\mathrm{aux}} = [-6, -1]$ for the hyperbolic cosine potential. For this case, we cannot use directly $\log_{10}(\lambda_{\phi i})$ because $\lambda_{\phi i} < 0$, so in order to cover the parameter space we use the auxiliary variable $\lambda_{\phi i,\mathrm{aux}}$ whose relation with $\lambda_{\phi i}$ is given by $\lambda_{\phi i} = -10^{-\lambda_{\phi i,\mathrm{aux}}}$. In what follows we will use $\mathrm{quad}_i$ to refer to the potential $V_i(\phi_i) = (1/2)m_{\phi i}^2\phi_i^2$, $\cos_i$ for $V_i(\phi_i) = m_{\phi i}^2 f_i^2\,[1 + \cos(\phi_i/f_i)]$ and $\cosh_i$ for $V_i(\phi_i) = m_{\phi i}^2 f_i^2\,[\cosh(\phi_i/f_i) - 1]$. If there is no subscript, it means that it is the single field case.

First, in Figure 4, we show the constraints for the single field cases, that is, the 1D marginalized posterior distribution of the free parameters for each model corresponding to the potentials $V(\phi) = 1/2m_\phi^2\phi^2$, $V(\phi) = m_\phi^2 f^2\,[1 + \cos(\phi/f)]$, and $V(\phi) = m_\phi^2 f^2\,[\cosh(\phi/f) - 1]$. It can be noticed that the posteriors of the field mass are very similar for the three potentials, and that the

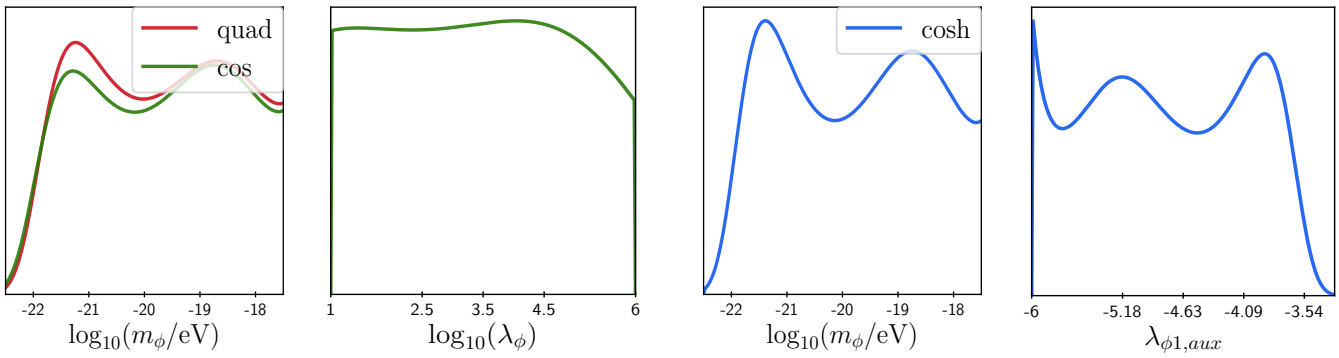



FIG. 4. 1D posterior distribution for the single SFDM with potentials $V(\phi) = 1/2m_\phi^2\phi^2$ (red), $V(\phi) = m_\phi^2 f^2\,[1 + \cos(\phi/f)]$ (green) and $V(\phi) = m_\phi^2 f^2\,[\cosh(\phi/f) - 1]$ (blue). The constraints on the field mass are very similar for the three potentials, whereas the self-interaction parameter $\lambda_\phi$ of the trigonometric potential remains unconstrained by the data.

[2] As mentioned in [49], the process of inferring the MPS is model-dependent, therefore we will consider the constraints obtained here as an approximation.

[3] See [57] for a bayesian inference review.

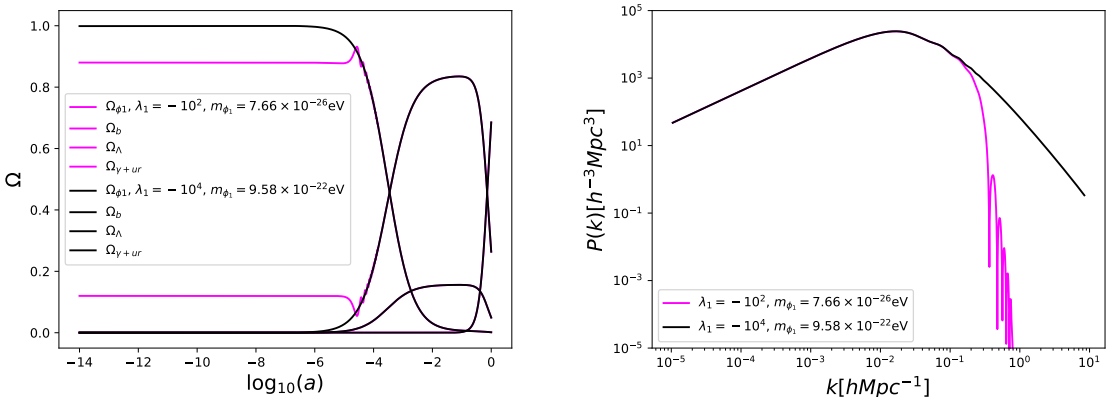



FIG. 5. Background and MPS evolution for the SFDM with potential $V(\phi) = m_\phi^2 f^2 \left[\cosh(\phi/f) - 1\right]$. Magenta lines correspond to $\lambda_\phi = -10^2$ with $m_\phi = 7.66 \times 10^{-26}$ eV, which are ruled out from the constraints obtained. We can see the scalar field contribution to radiation. On the other hand, black lines, that correspond to $\lambda_\phi = -10^4$ with $m_\phi = 9.58 \times 10^{-22}$ eV, represent values within the confidence regions.

observations considered can only put a lower bound on it, which is $\log(m_\phi/\text{eV}) \gtrsim -21.9$ at 95% CL for the quadratic and hyperbolic cosine potentials and $\log(m_\phi/\text{eV}) \gtrsim -21.8$ at 95% CL for the trigonometric cosine potential. In the case of the trigonometric potential, we see that its extra parameter $\lambda_\phi$ appears unconstrained and the posterior looks practically the same with the prior we considered above for this parameter, which is consistent with previous studies [23, 33, 34]. As for the hyperbolic cosine, we have already mentioned the close relationship between the field mass $m_\phi$ and the self-interaction parameter $\lambda_\phi$, and then the constraints on the former are translated to $\log(-\lambda_\phi) \gtrsim 3.6$ at 95% CL. The excluded values of $\lambda_\phi$ correspond to the cases in which SFDM has a significant contribution as an early radiation component. An example of this can be seen in Figure 5.

For completeness, we also present in Fig. 6 the 1D posterior distributions for the cosmological common parameters of the models: the density parameters (SFDM and $\Lambda$), and the Hubble constant $H_0$. The posteriors are very similar for the three models, which show that one recovers the results of the standard $\Lambda$CDM model.

In Fig. 7 we show the posteriors for the combinations $V(\phi_1) = 1/2 m_{\phi 1}^2 \phi_1^2$ with $V(\phi_2) = 1/2 m_{\phi 2}^2 \phi_2^2$, $V(\phi_1) = 1/2 m_{\phi 1}^2 \phi_1^2$ with $V(\phi_2) = m_{\phi 2}^2 f^2 \left[1 + \cos(\phi_2/f)\right]$ and $V(\phi_{1,2}) = m_{\phi 1,2}^2 f^2 \left[1 + \cos(\phi_{1,2}/f)\right]$. For the quadratic-quadratic and quadratic-cos combinations we found a lower bound for the mass of both fields given by $\log_{10}(m_{\phi 1,2}/\text{eV}) = -22.1$ at 95%. While, for the cos-cos combination, the lower bound for the mass of field one is $\log_{10}(m_{\phi 1}/\text{eV}) = -22.1$ at 95% and for the second field $\log_{10}(m_{\phi 2}/\text{eV}) = -22.2$ at 95%. We also found that the density parameter $\Omega_{\phi i}$ of one field depends

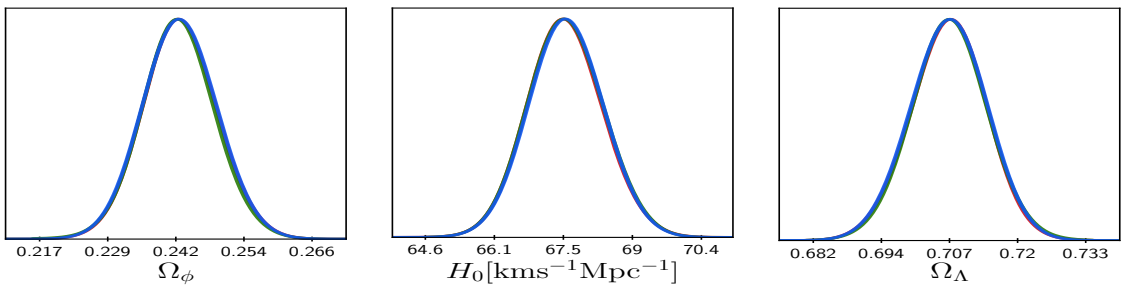



FIG. 6. 1D posterior distribution for the cosmological common parameters of all the models studied in this work.

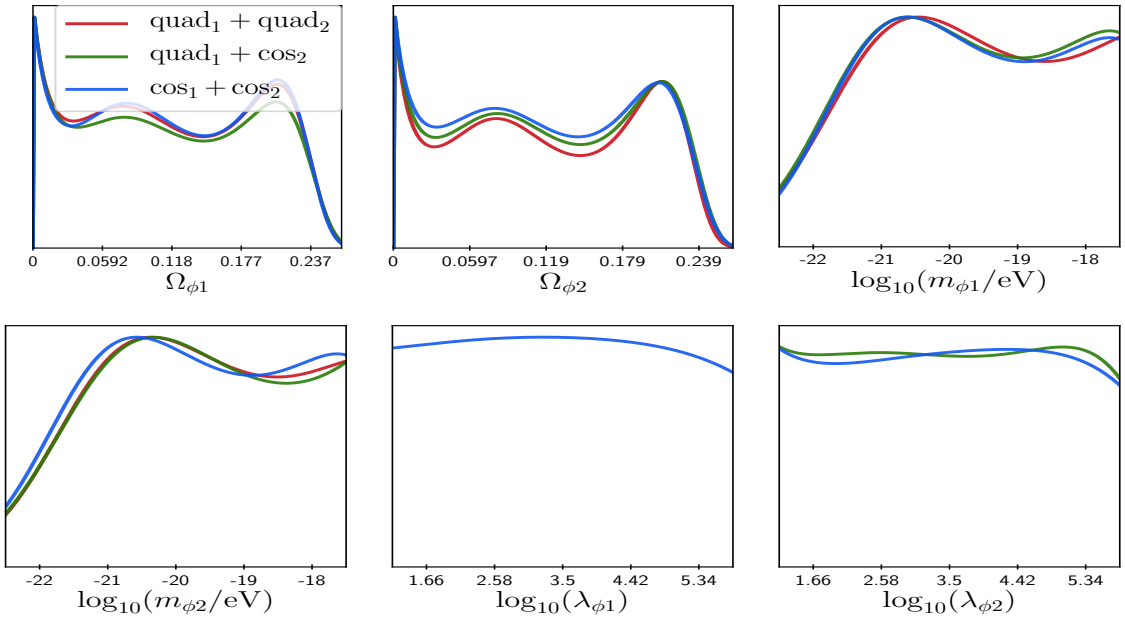



FIG. 7. 1D posterior distribution for the two SFDM with the potentials $V(\phi_{1,2}) = 1/2m^2_{\phi 1,2}\phi^2_{1,2}$ (red), $V(\phi_1) = 1/2m^2_{\phi 1}\phi^2_1$ with $V(\phi_1) = m^2_{\phi 1}f^2\left[1+\cos(\phi_1/f)\right]$ (green) and $V(\phi_{1,2}) = m^2_{\phi 1,2}f^2\left[1+\cos(\phi_{1,2}/f)\right]$ (blue).

on the $\Omega_{\phi j}$ of the other field. That is, if $\Omega_{\phi 1}$ dominates then $\Omega_{\phi 2}$ is small, and on the other way around because the total contribution remains constant. In [40] the authors propose two scalar fields (with the possibility of a third one) with masses $m_{\phi 1} \approx 10^{-22}$ eV and $m_{\phi 2} \approx 10^{-20}$ eV, and these values are within our confidence regions. The fact that the lighter field dominates over the massive field is also in agreement with our results.

To assess any preference of the observational data for MSFDM models, we compute the Bayes factor, $\ln \mathcal{B}_{i,j}$, by using the numerical package MCEvidence [58], and the ratio is done respect to CDM. The results are shown in Table I. Following the Jeffreys guideline [57], if $\ln \mathcal{B}_{i,j} > 5$ we have a decisive strength against model $i$; if $5 > \ln \mathcal{B}_{i,j} > 2.5$ it means a strong strength; if $2.5 > \ln \mathcal{B}_{i,j} > 1$ we have a significant strength and if $\ln \mathcal{B}_{i,j} < 1$ the data prefers model $i$. In general, we should be careful taking the values of the Bayes factor since some of the parameters were unconstrained by the data. However, bearing in mind this point, we obtain that models with two scalar fields get penalized because the addition of the extra parameters. But for the *cosh* potential, where the MPS presents a bump, the Bayes factor seems to provide a good evidence in favour of this model, even though it has one extra degree of freedom. Despite all the scalar field combinations are penalized through the Bayes' factor, the minimum of the likelihoods correspond to the same value $-\ln \mathcal{L}_{\min} = 523.03$. That is, we can find a suitable combination of parameters such that the model in place resembles the behaviour of a cold dark matter.

| | quad | cos | cosh | quad$_1$ + quad$_2$ | quad$_1$ + cos$_2$ | cos$_1$ + cos$_2$ |
|---|---|---|---|---|---|---|
| $\ln \mathcal{B}_{i,\Lambda\mathrm{CDM}}$ | 1.59 | 3.3 | 0.85 | 2.13 | 3.74 | 5.68 |

TABLE I. Bayes factor for SFDM and double-SFDM with different potentials using ΛCDM as reference.

## 4. CONCLUSIONS

In this paper we presented the cosmological constraints of the Multi Scalar Field Dark Matter (MSFDM) model, in which we assume the dark matter is composed of different ultralight scalar fields. The idea was introduced to alleviate some of the cosmological and astrophysical discrepancies, for instance, the distinct values of the single scalar field mass obtained when considering different observations, where more than one field is needed in order to explain them. As a first approximation, we took for granted that the scalar fields are real, spatially homogeneous and they do not interact with each other. We presented the equations that describe the evolution of the background and perturbations for $N$ scalar fields, and by using the polar change of variables we avoided the scalar field characteristic oscillations. Thus, we obtained a general expression for the fields evolution that depend on the potential and its derivatives, in particular, the equations for the potentials $V(\phi) = 1/2m_\phi^2\phi^2$, $V(\phi) = m_\phi^2 f^2\left[1+\cos(\phi/f)\right]$ and $V(\phi) = m_\phi^2 f^2\left[\cosh(\phi/f)-1\right]$. Under this change of variables, these three configurations are described by a single system of equations where the parameter $\lambda_\phi$ is able to decide the type of potential to use.

We showed the evolution for the background, mass power spectrum (MPS) and the CMB power spectrum using a modify version of the CLASS code [18, 22, 50] with two dark matter components. We considered the following combinations: a) cold dark matter and a scalar field with potential $V(\phi) = 1/2m_\phi^2\phi^2$, and two scalar field models, with b) both potentials $V(\phi) = 1/2m_\phi^2\phi^2$, c) $V(\phi) = 1/2m_\phi^2\phi^2$ and $V(\phi) = m_\phi^2 f^2\left[1+\cos(\phi/f)\right]$, and d) $V(\phi) = 1/2m_\phi^2\phi^2$ and $V(\phi) = m_\phi^2 f^2\left[\cosh(\phi/f)-1\right]$. Since the fields are independent from each other, we introduced the parameter $R$ to have the field one as reference. We showed that the evolution of the background is mainly affected at the beginning of the scalar fields oscillations since its amplitude depends on the masses and the contribution that each one has to the total dark matter, being bounded by the heaviest and lightest masses; however these do not depend on $\lambda_\phi$. After the oscillations have started, the fields evolution only depend on $\Omega_{\phi i,0}$. On the other hand we found that, in all combinations, the MPS presents the characteristic cut-off of the single field at small scales. However, it does not present the oscillations of the single case due to the superposition of the different fields. This cut-off is far form the $\Lambda$CDM behavior when the lightest field dominates, and if the heaviest one dominates the MPS behavior approaches the $\Lambda$CDM model. For the case that one of the fields has the axion potential, the characteristic bump appeared when it had a light mass with large $\lambda_\phi$ values. On the contrary, if the mass is heavier, the bump disappeared regardless of the values of $\lambda_\phi$ and $R$. On the other hand, in the CMB power spectrum, we have not found significant changes unless one of the fields has $m_{\phi i} \leq 10^{-26}$ eV. That is, regardless of the number of fields we can always find a combination of the fields that matches the CMB observationsm where the total contribution of dark matter is $\Omega_{\rm DM} = 0.264$, given by Planck 18 data [59].

We performed the parameter inference analysis with the Monte Python code [60, 61] using BAO, Big Bang Nucleosynthesis, Ly-$\alpha$ forest and Supernovae for a single scalar field with the three potentials mentioned above and for double scalar fields. In the latter case, for simplicity we used the following combination of potentials: $V(\phi_1) = 1/2m_{\phi 1}^2\phi_1^2$ with $V(\phi_2) = 1/2m_{\phi 2}^2\phi_2^2$, $V(\phi_1) = 1/2m_{\phi 1}^2\phi_1^2$ with $V(\phi_2) = m_{\phi 2}^2 f^2\left[1+\cos(\phi_2/f)\right]$ and $V(\phi_1) = m_{\phi 1}^2 f^2\left[1+\cos(\phi_1/f)\right]$ with $V(\phi_2) = m_{\phi 2}^2 f^2\left[1+\cos(\phi_2/f)\right]$. For the single case we found a bound for the mass values that corresponds to the one reported by the Ly-$\alpha$ data. We also presented the constrictions for the potential $V(\phi) = m_\phi^2 f^2\left[\cosh(\phi/f)-1\right]$ where we have found a bound for $\lambda_\phi$ and, therefore, for the scalar field mass where, the latter, is also in agreement with the reported by the Ly-$\alpha$. In this case, the excluded values correspond to the cases in which the scalar field contributes to radiation as can be seen in Figure 5. For the double field models we found bounds for the masses and that the contribution of the fields depends on each other. Within our confidence regions are the masses

reported in [40], in which more than one scalar fields is needed to explain the observed galaxies halos.

Finally, we have found that adding more scalar fields in order to explain astrophysical phenomena does not affect the known cosmology. So the MSFDM can be an alternative candidate to dark matter that is able to explain the observations at the cosmological and astrophysical levels. Its difference with other models is seen in the MPS at small scales. The results presented here can be generalized to larger number of fields with different potentials. We expect that forthcoming observations of collaborations such as DESI and LSST will allow us to better constrain the parameters of our model.

## ACKNOWLEDGMENTS

The authors thank Luis Ureña for the long and productive discussions about the paper. L.O.T.T acknowledge financial support from CONACyT doctoral fellowship. J.A.V. acknowledges the support provided by FOSEC SEP-CONACYT Investigación Básica A1-S-21925 and UNAM-DGAPA-PAPIIT IA104221. This work was partially supported by CONACyT México under grants A1-S-8742, 304001, 376127, 240512; The authors are gratefully for the computing time granted by LANCAD and CONACYT in the Supercomputer Hybrid Cluster "Xiuhcoatl" at GENERAL COORDINATION OF INFORMATION AND COMMUNICATIONS TECHNOLOGIES (CGSTIC) of CINVESTAV. URL: https://clusterhibrido.cinvestav.mx/ and Abacus clusters at Cinvestav, IPN; I0101/131/07 C-234/07 of the Instituto Avanzado de Cosmología (IAC) collaboration (http://www.iac.edu.mx/).

[1] D.H. Weinberg, J.S. Bullock, F. Governato, R. Kuzio de Naray and A.H.G. Peter, *Cold dark matter: controversies on small scales*, *Proc. Nat. Acad. Sci.* **112** (2015) 12249 [1306.0913].

[2] P. Bull et al., *Beyond ΛCDM: Problems, solutions, and the road ahead*, *Phys. Dark Univ.* **12** (2016) 56 [1512.05356].

[3] S.-J. Sin, *Late-time phase transition and the galactic halo as a bose liquid*, *Phys. Rev. D* **50** (1994) 3650.

[4] J.-w. Lee and I.-g. Koh, *Galactic halos as boson stars*, *Phys. Rev. D* **53** (1996) 2236 [hep-ph/9507385].

[5] F. Guzman, T. Matos and H. Villegas, *Scalar fields as dark matter in spiral galaxies: comparison with experiments*, *Astronomische Nachrichten* **320** (1999) 97.

[6] T. Matos and F.S. Guzman, *Scalar fields as dark matter in spiral galaxies*, *Class. Quant. Grav.* **17** (2000) L9 [gr-qc/9810028].

[7] W. Hu, R. Barkana and A. Gruzinov, *Cold and fuzzy dark matter*, *Phys. Rev. Lett.* **85** (2000) 1158 [astro-ph/0003365].

[8] C.G. Boehmer and T. Harko, *Can dark matter be a Bose-Einstein condensate?*, *JCAP* **06** (2007) 025 [0705.4158].

[9] L. Hui, J.P. Ostriker, S. Tremaine and E. Witten, *Ultralight scalars as cosmological dark matter*, *Phys. Rev. D* **95** (2017) 043541 [1610.08297].

[10] T. Matos and F.S. Guzman, *Scalar fields as dark matter in spiral galaxies*, *Class. Quant. Grav.* **17** (2000) L9 [gr-qc/9810028].

[11] J. Magaña and T. Matos, *A brief Review of the Scalar Field Dark Matter model*, in *Journal of Physics Conference Series*, vol. 378 of *Journal of Physics Conference Series*, p. 012012, Aug., 2012, DOI [1201.6107].

[12] T. Matos, A. Vazquez-Gonzalez and J. Magana, $\phi^2$ *as Dark Matter*, *Mon. Not. Roy. Astron. Soc.* **393** (2009) 1359 [0806.0683].

[13] A. Suárez, V.H. Robles and T. Matos, *A Review on the Scalar Field/Bose-Einstein Condensate Dark Matter Model*, *Astrophys. Space Sci. Proc.* **38** (2014) 107 [1302.0903].

[14] L.A. Ureña López, *Brief Review on Scalar Field Dark Matter Models*, *Front. Astron. Space Sci.* **6** (2019) 47.

[15] L.E. Padilla, J.A. Vázquez, T. Matos and G. Germán, *Scalar Field Dark Matter Spectator During Inflation: The Effect of Self-interaction*, *JCAP* **05** (2019) 056 [1901.00947].

[16] A. Navarro-Boullosa, A. Bernal-Bautista and J. Vazquez, *Bayesian analysis for rotational curves with $\ell$-boson stars as a dark matter component*, In preparation.

[17] T. Matos, A. Vazquez-Gonzalez and J. Magana, *Study of several potentials as scalar field dark matter candidates*, *AIP Conf. Proc.* **1083** (2008) 144.

[18] L.A. Ureña López and A.X. Gonzalez-Morales, *Towards accurate cosmological predictions for rapidly oscillating scalar fields as dark matter*, *JCAP* **07** (2016) 048 [1511.08195].

[19] B. Li, T. Rindler-Daller and P.R. Shapiro, *Cosmological Constraints on Bose-Einstein-Condensed Scalar Field Dark Matter*, *Phys. Rev. D* **89** (2014) 083536 [1310.6061].

[20] A. Suárez and P.-H. Chavanis, *Hydrodynamic representation of the Klein-Gordon-Einstein equations in the weak field limit: General formalism and perturbations analysis*, *Phys. Rev. D* **92** (2015) 023510 [1503.07437].

[21] A. Suárez and P.-H. Chavanis, *Cosmological evolution of a complex scalar field with repulsive or attractive self-interaction*, *Phys. Rev. D* **95** (2017) 063515 [1608.08624].

[22] F.X.L. Cedeño, A.X. González-Morales and L.A. Ureña López, *Cosmological signatures of ultralight dark matter with an axionlike potential*, *Phys. Rev. D* **96** (2017) 061301 [1703.10180].

[23] F.X. Linares Cedeño, A.X. González-Morales and L.A. Ureña López, *Ultralight DM bosons with an axion-like potential: scale-dependent constraints revisited*, *JCAP* **01** (2021) 051 [2006.05037].

[24] G.G. Ross, G. German and J.A. Vazquez, *Hybrid Natural Inflation*, *JHEP* **05** (2016) 010 [1601.03221].

[25] T. Matos, J.-R. Luevano, I. Quiros, L.A. Ureña Lopez and J.A. Vazquez, *Dynamics of scalar field dark matter with a cosh-like potential*, *Physical Review D* **80** (2009) .

[26] L.A. Ureña López, *Scalar field dark matter with a cosh potential, revisited*, *JCAP* **06** (2019) 009 [1904.03318].

[27] R. Hlozek, D. Grin, D.J.E. Marsh and P.G. Ferreira, *A search for ultralight axions using precision cosmological data*, *Phys. Rev. D* **91** (2015) 103512 [1410.2896].

[28] A. Paredes and H. Michinel, *Interference of Dark Matter Solitons and Galactic Offsets*, *Phys. Dark Univ.* **12** (2016) 50 [1512.05121].

[29] A.X. González-Morales, D.J.E. Marsh, J. Peñarrubia and L.A. Ureña López, *Unbiased constraints on ultralight axion mass from dwarf spheroidal galaxies*, *Mon. Not. Roy. Astron. Soc.* **472** (2017) 1346 [1609.05856].

[30] V. Lora, J. Magana, A. Bernal, F.J. Sanchez-Salcedo and E.K. Grebel, *On the mass of ultra-light bosonic dark matter from galactic dynamics*, *JCAP* **02** (2012) 011 [1110.2684].

[31] E. Calabrese and D.N. Spergel, *Ultra-Light Dark Matter in Ultra-Faint Dwarf Galaxies*, *Mon. Not. Roy. Astron. Soc.* **460** (2016) 4397 [1603.07321].

[32] A. Sarkar, R. Mondal, S. Das, S.K. Sethi, S. Bharadwaj and D.J.E. Marsh, *The effects of the small-scale DM power on the cosmological neutral hydrogen (HI) distribution at high redshifts*, *JCAP* **04** (2016) 012 [1512.03325].

[33] E. Armengaud, N. Palanque-Delabrouille, C. Yèche, D.J.E. Marsh and J. Baur, *Constraining the mass of light bosonic dark matter using SDSS Lyman-$\alpha$ forest*, *Mon. Not. Roy. Astron. Soc.* **471** (2017) 4606 [1703.09126].

[34] V. Iršič, M. Viel, M.G. Haehnelt, J.S. Bolton and G.D. Becker, *First constraints on fuzzy dark matter from Lyman-$\alpha$ forest data and hydrodynamical simulations*, *Phys. Rev. Lett.* **119** (2017) 031302 [1703.04683].

[35] D.J.E. Marsh, *Axion Cosmology*, *Phys. Rept.* **643** (2016) 1 [1510.07633].

[36] P. Mocz et al., *First star-forming structures in fuzzy cosmic filaments*, *Phys. Rev. Lett.* **123** (2019) 141301 [1910.01653].

[37] O. Müller, M.S. Pawlowski, H. Jerjen and F. Lelli, *A whirling plane of satellite galaxies around Centaurus A challenges cold dark matter cosmology*, *Science* **359** (2018) 534 [1802.00081].

[38] L.E. Strigari, J.S. Bullock, M. Kaplinghat, J.D. Simon, M. Geha, B. Willman et al., *A common mass scale for satellite galaxies of the Milky Way*, *Nature* **454** (2008) 1096 [0808.3772].

[39] A. Arvanitaki, S. Dimopoulos, S. Dubovsky, N. Kaloper and J. March-Russell, *String Axiverse*, *Phys. Rev. D* **81** (2010) 123530 [0905.4720].

[40] H.N. Luu, S.H.H. Tye and T. Broadhurst, *Multiple Ultralight Axionic Wave Dark Matter and Astronomical Structures*, *Phys. Dark Univ.* **30** (2020) 100636 [1811.03771].

[41] A. Paliathanasis and M. Tsamparlis, *Two scalar field cosmology: Conservation laws and exact solutions*, *Phys. Rev. D* **90** (2014) 043529 [1408.1798].

[42] J.A. Vázquez, D. Tamayo, A.A. Sen and I. Quiros, *Bayesian model selection on scalar $\epsilon$-field dark energy*, *Phys. Rev. D* **103** (2021) 043506 [2009.01904].

[43] D. Benisty and E.I. Guendelman, *Two scalar fields inflation from scale-invariant gravity with modified measure*, *Class. Quant. Grav.* **36** (2019) 095001 [1809.09866].

[44] K. Bamba, S.D. Odintsov and P.V. Tretyakov, *Inflation in a conformally-invariant two-scalar-field theory with an extra $R^2$ term*, *Eur. Phys. J. C* **75** (2015) 344 [1505.00854].

[45] J.A. Vázquez, L.E. Padilla and T. Matos, *Inflationary Cosmology: From Theory to Observations*, 1810.09934.

[46] O. Bertolami, P. Carrilho and J. Paramos, *Two-scalar-field model for the interaction of dark energy and dark matter*, *Phys. Rev. D* **86** (2012) 103522 [1206.2589].

[47] E. Gutiérrez-Luna, B. Carvente, V. Jaramillo, J. Barranco, C. Escamilla-Rivera, C. Espinoza et al., *Scalar field dark matter with two components: combined approach from particle physics and cosmology*, 2110.10258.

[48] L.A. Ureña López, *New perturbative method for analytical solutions in single-field models of inflation*, *Phys. Rev. D* **94** (2016) 063532 [1512.07142].

[49] S. Chabanier, M. Millea and N. Palanque-Delabrouille, *Matter power spectrum: from Ly$\alpha$ forest to CMB scales*, *Mon. Not. Roy. Astron. Soc.* **489** (2019) 2247 [1905.08103].

[50] D. Blas, J. Lesgourgues and T. Tram, *The cosmic linear anisotropy solving system (class). part ii: Approximation schemes*, *Journal of Cosmology and Astroparticle Physics* **2011** (2011) 034–034.

[51] https://github.com/losvaldote/two_sfdm_class.

[52] A. Cuceu, J. Farr, P. Lemos and A. Font-Ribera, *Baryon Acoustic Oscillations and the Hubble Constant: Past, Present and Future*, *JCAP* **10** (2019) 044 [1906.11628].

[53] BOSS collaboration, *The clustering of galaxies in the completed SDSS-III Baryon Oscillation Spectroscopic Survey: cosmological analysis of the DR12 galaxy sample*, *Mon. Not. Roy. Astron. Soc.* **470** (2017) 2617 [1607.03155].

[54] F. Beutler, C. Blake, M. Colless, D.H. Jones, L. Staveley-Smith, L. Campbell et al., *The 6df galaxy survey: baryon acoustic oscillations and the local hubble constant*, *Monthly Notices of the Royal Astronomical Society* **416** (2011) 3017–3032.

[55] A.J. Ross, L. Samushia, C. Howlett, W.J. Percival, A. Burden and M. Manera, *The clustering of the SDSS DR7 main Galaxy sample – I. A 4 per cent distance measure at $z = 0.15$*, *Mon. Not. Roy. Astron. Soc.* **449** (2015) 835 [1409.3242].

[56] D.M. Scolnic et al., *The Complete Light-curve Sample of Spectroscopically Confirmed SNe Ia from Pan-STARRS1 and Cosmological Constraints from the Combined Pantheon Sample*, *Astrophys. J.* **859** (2018) 101 [1710.00845].

[57] L.E. Padilla, L.O. Tellez, L.A. Escamilla and J.A. Vazquez, *Cosmological Parameter Inference with Bayesian Statistics*, *Universe* **7** (2021) 213 [1903.11127].

[58] A. Heavens, Y. Fantaye, A. Mootoovaloo, H. Eggers, Z. Hosenie, S. Kroon et al., *Marginal Likelihoods from Monte Carlo Markov Chains*, *arXiv e-prints* (2017) arXiv:1704.03472 [1704.03472].

[59] http://pla.esac.esa.int/pla/#home.

[60] T. Brinckmann and J. Lesgourgues, *MontePython 3: boosted MCMC sampler and other features*, *Phys. Dark Univ.* **24** (2019) 100260 [1804.07261].

[61] B. Audren, J. Lesgourgues, K. Benabed and S. Prunet, *Conservative constraints on early cosmology with montepython*, *Journal of Cosmology and Astroparticle Physics* **2013** (2013) 001–001.